Axial Sloshing of Liquid Hydrogen at low Bond Numbers with Different Wall Superheat

Michael E. Dreyer

with Peter Friese, Malte Koppe,
Niklas Weber, Sergey Zhemchuzhin

Department of Fluid Mechanics (DFM)
Faculty of Production Engineering
- Mechanical Engineering and Process Engineering -
University of Bremen

ZARM, Am Fallturm 2, 28359 Bremen
michael.dreyer@zarm.uni-bremen.de

Bremen — October 25, 2019

Axial sloshing at low Bond numbers is initiated by a step reduction of the gravitational (or any other) acceleration to very low values. The Bond number compares the hydrostatic pressure with the capillary pressure, or the characteristic length L_c of the container with the capillary length L_L or Laplace length:

$$\mathrm{Bo} = \frac{(\rho_L - \rho_G)\, a_c L_c^2}{\sigma} = \frac{L_c^2}{L_L^2} \tag{1}$$

The free surface oscillates around its final equilibrium shape after a reorientation from the high Bo shape to a constant curvature shape. The oscillation may also be triggered by disturbances in an otherwise fully compensated gravity environment. The boundary condition is the microscopic contact angle θ_{mic} which is zero for liquid hydrogen in contact with Pyrex glass (and other solid as well).

The static interface for $\mathrm{Bo} \to 0$ has a hemispherical shape, with the radius of the container as the sphere radius. A liquid film at the wall exists which will be discussed later.

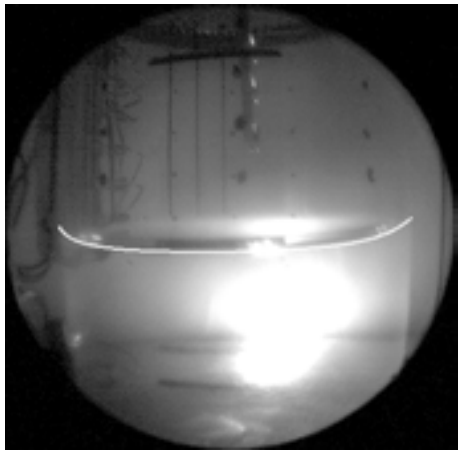

(a) Initial

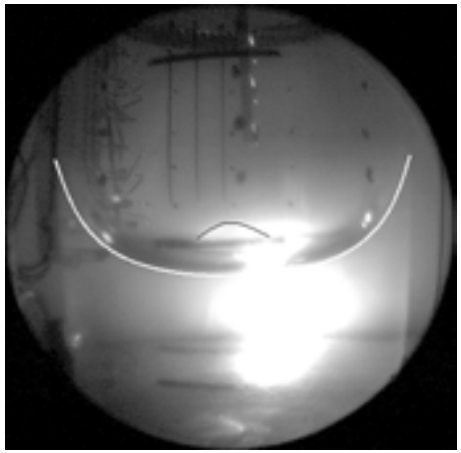

(b) Capillary wave

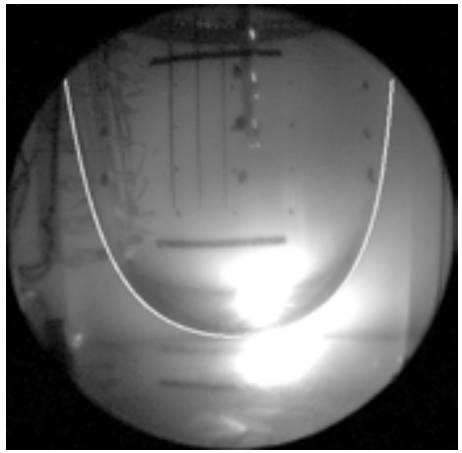

(c) 1st minimum

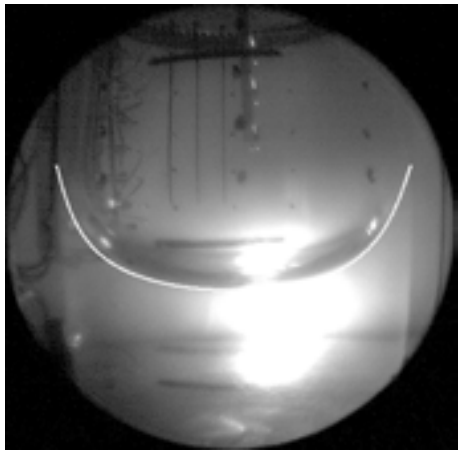

(d) 1st maximum

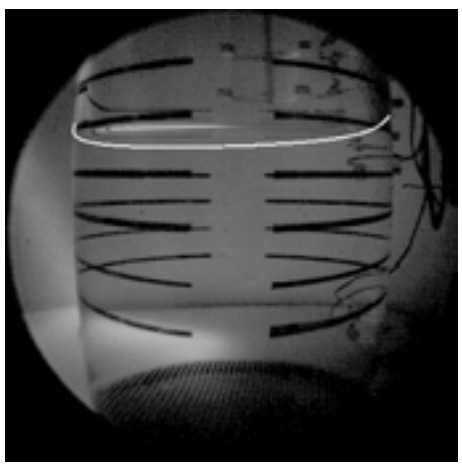

(e) Initial

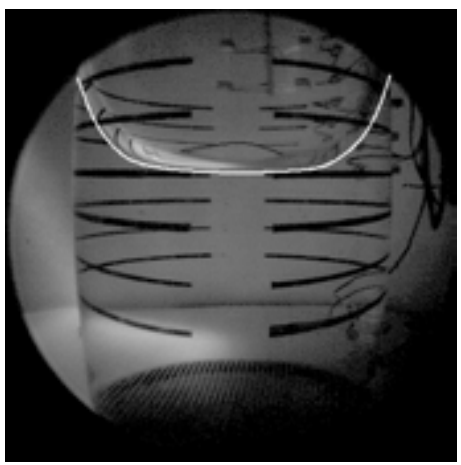

(f) Capillary wave

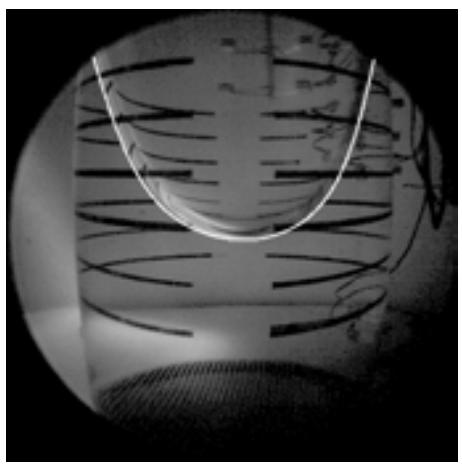

(g) 1st minimum

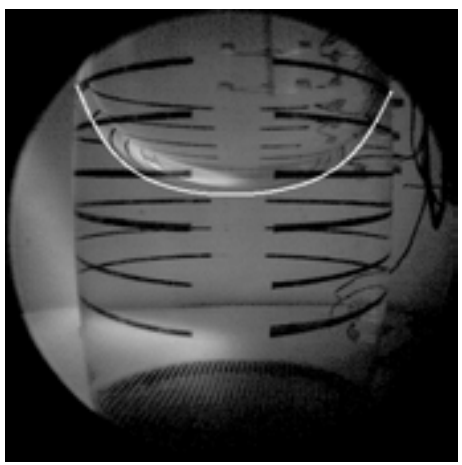

(h) 1st maximum

Figure 1: $R = 26.2\,\text{mm}$ top row, $R = 20.15\,\text{mm}$ bottom row. Show video!

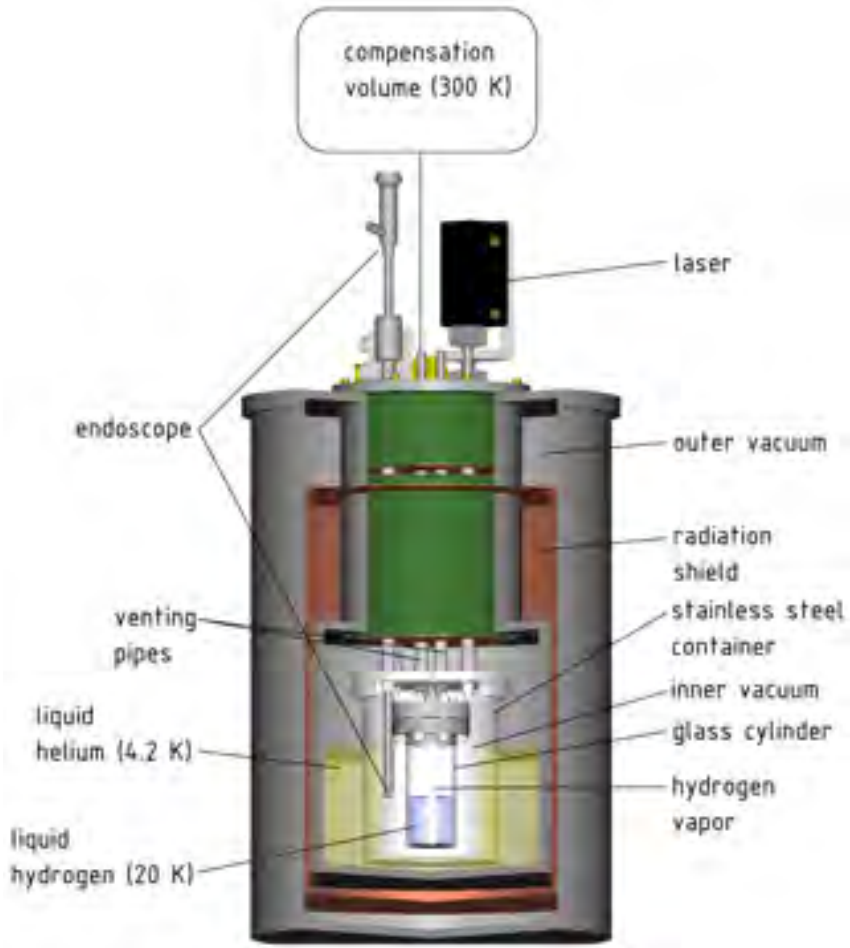

(a) Cryostat

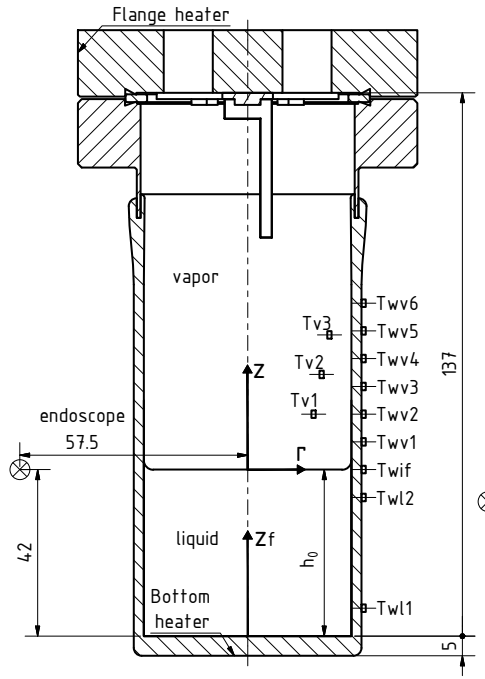

(b) Setup *I* dimensions

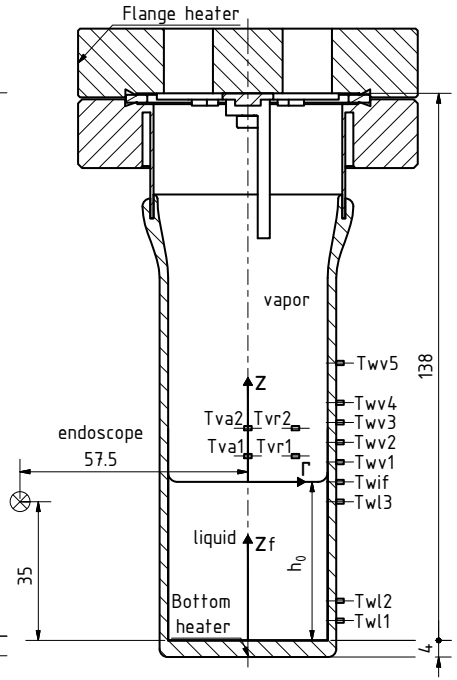

(c) Setup *II* dimensions

Figure 2: (a) Cryostat, (b) Experiment setup: $R = 26.2\,\text{mm}$, wall thickness $2.6\,\text{mm}$, (c) $R = 20.15\,\text{mm}$, wall thickness $2.2\,\text{mm}$

Some basics facts about axial sloshing:

1. Bounded free surface oscillations are basic problems of fluid mechanics. No analytical solutions are available for viscous liquids which are perfectly wetting, such as cryogenic liquids.
2. Analytical solutions are based on potential flow assumptions (inviscid, irrotational), small amplitudes, and contact angles $0.2\pi \leq \theta \leq 0.8\pi$ (see Bauer and Eidel 1990[1]).
3. Sloshing of any kind has early been investigated by NASA and other space faring nations. Axial sloshing may occur at the end of thrust and the beginning of a ballistic phase (see Siegert et al. 1964[2]).
4. Sloshing is a test problem for the validation of computational fluid dynamics (CFD) tools.

[1] Bauer H. F. and Eidel W. (1990), Linear liquid oscillations in a cylindrical container under zero gravity, Appl. Microgravity Tech. II 4, 212-220.

[2] Siegert C. E., Petrash D. A., and Otto E. W., Time response of liquid-vapor interface after entering weightlessness, NASA TN D-2458

The free surface contour is described by $\eta(r,t)$. We assume cylindrical symmetry. The wall point is at

$$\eta(R,0) = H_\mathrm{L} + L_\mathrm{L}\left[2\left(1-\sin\theta\right)\right]^{1/2} \tag{2}$$

with the LAPLACE length

$$L_\mathrm{L} = \left(\frac{\sigma}{\rho_\mathrm{L} g_\mathrm{E}}\right)^{1/2} \tag{3}$$

Assuming a constant volume of liquid (no correction for the meniscus or the film), the low Bo contour has a hemispherical shape with the coordinates $\eta(0,\infty) = H_\mathrm{L} - R/3$ and $\eta(R,\infty) = H_\mathrm{L} + 2R/3$ for $\theta = 0$.

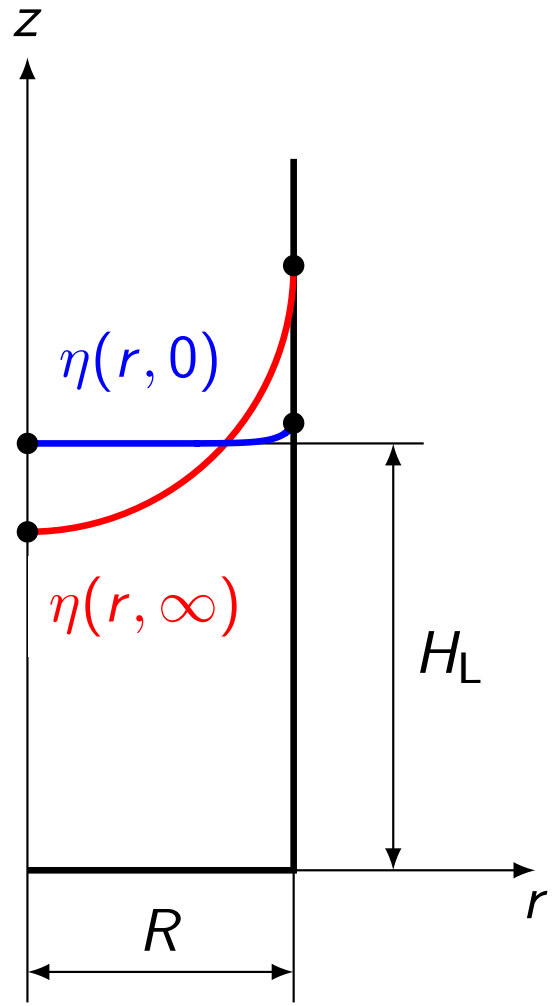

Figure 3: Initial $\eta(r,0)$ and final $\eta(r,\infty)$ interface contour

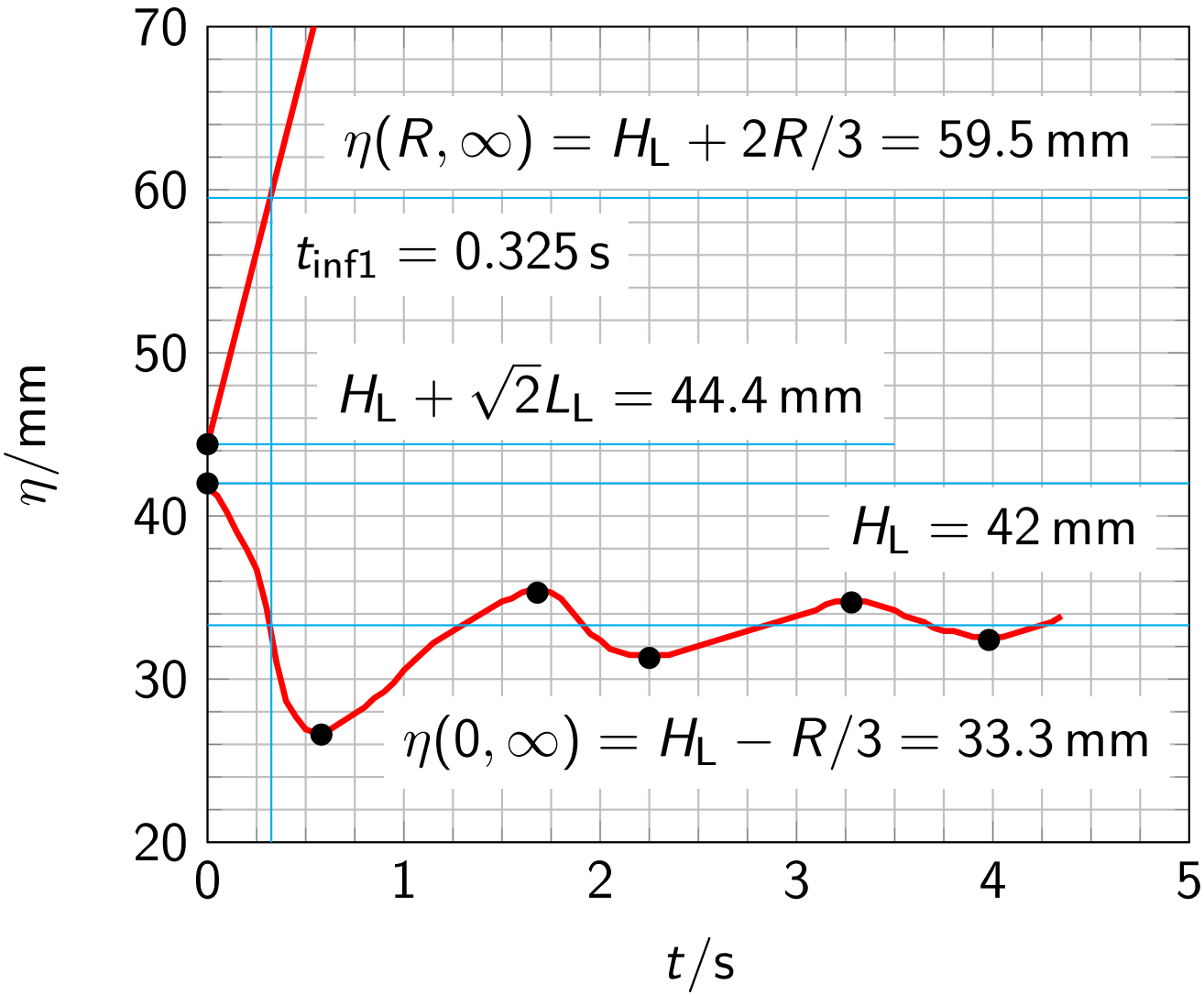

Figure 4: Surface elevation $\eta(r = R, t)$ (top left) and $\eta(r = 0, t)$ (bottom) for a test with $R = 26.2\,\text{mm}$ (A05: $p = 95\,005\,\text{Pa}$, $T_{\text{sat}} = 20.056\,\text{K}$)

Table 1: Thermophysical properties of para-hydrogen p-H_2 at normal boiling point (NBP) conditions $p = 101.325\,\mathrm{kPa}$, saturation temperature is $T_{sat} = 20.27\,\mathrm{K}$. Critical temperature is $T_{crit} = 32.94\,\mathrm{K}$, and $T_{sat}/T_{crit} = 0.62$.

		liquid	gas	Pyrex
ρ	$\mathrm{kg\,m^{-3}}$	70.83	1.34	2214
μ	$10^{-6}\,\mathrm{Pa\,s}$	13.50	1.00	
ν	$10^{-6}\,\mathrm{m^2\,s^{-1}}$	0.19	0.74	
σ	$10^{-3}\,\mathrm{N\,m^{-1}}$	1.91		
λ	$10^{-3}\,\mathrm{W\,m^{-1}\,K^{-1}}$	100.6	16.7	150.0
c_p	$\mathrm{kJ\,kg^{-1}\,K^{-1}}$	9.73	12.03	30.60
D_T	$10^{-6}\,\mathrm{m^2\,s^{-1}}$	0.15	1.10	2.21
$(\triangle_{LG} h)$	$\mathrm{kJ\,kg^{-1}}$	446.07		

$\mathrm{Ka} = 1114$, $\mathrm{Oh}(L_c = R = 26.2\,\mathrm{mm}) = 2 \times 10^{-4}$

The Laplace length is

$$L_\mathrm{L} = 1.68\,\mathrm{mm} \qquad (15)$$

The meniscus height at the wall is

$$\eta(R, 0) = 2.37\,\mathrm{mm} \qquad (16)$$

With the step reduction of the Bo number, the pressure in the wall region drives the leading edge upwards. Scaling velocity $v_{\mathrm{c}1}$ is

$$v_{\mathrm{c}1}(\sqrt{2}L_\mathrm{L}) = 108\,\mathrm{mm\,s^{-1}} \qquad (17)$$

We observed leading edge velocities of $(75 \pm 5)\,\mathrm{mm\,s^{-1}}$ for isothermal experiments, and $(50 \pm 5)\,\mathrm{mm\,s^{-1}}$ for superheated walls ($t < 0.1\,\mathrm{s}$).

The process is driven by inertia and leaves a film on the wall. We could not observe the film in our experiments, but all numerical calculations show the film which is several millimeters thick.

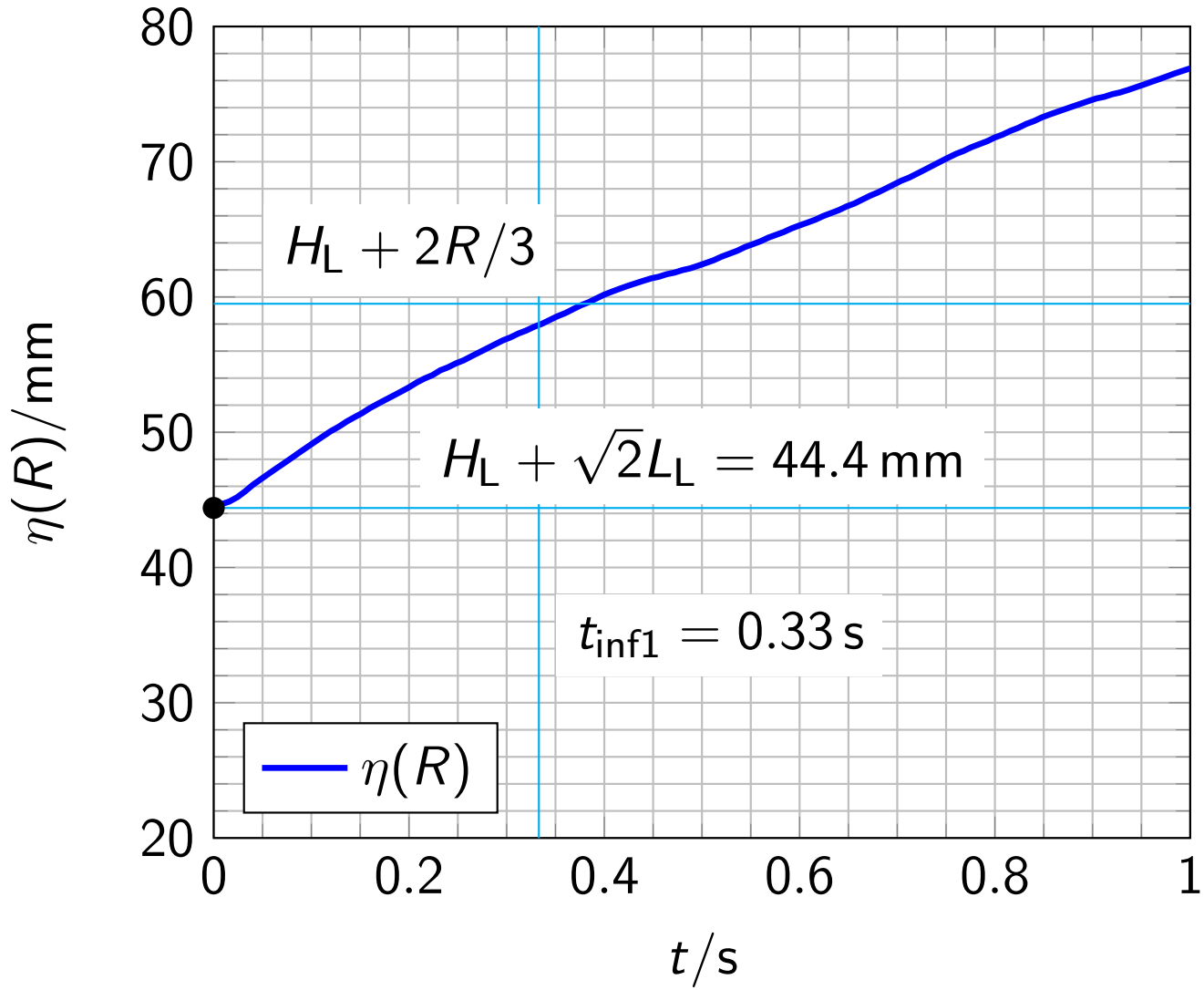

Figure 6: Surface elevation $\eta(r = R, t)$ from a numerical calulation (case A05) with 100 µm mesh resolution. The leading edge overshoots the final wall height by far.

Modal analysis under zero gravity for a 90° contact angle predicts (see Ibrahim 2005, p. 764[5]) the dispersion relation

$$\omega_{mn}^2 = \frac{\sigma}{\rho_L R^3}\epsilon_{mn}^3 \tanh\left(\epsilon_{mn}\frac{H_L}{R}\right) = \frac{\sigma}{\rho_L}k_{01}^3 \tanh\left(k_{01}H_L\right) \tag{26}$$

The eigenvalues ϵ_{mn} are the n-th zero points of the derivative of the Bessel function of first kind and order m. The first axial slosh mode has $m = 0$ waves around the circumference (symmetric) and $n = 1$ wave along the diameter. The liquid height is denoted with H_L. The tanh goes to unity for large arguments, therefor the bottom influence vanishes for a liquid depth ratio of

$$\frac{H_L}{R} \geq 0.5 \tag{27}$$

for the (0,1) mode. The eigenvalue is $\epsilon_{01} = 3.832$, and the wave number is $k_{01}R = 3.832$. With this, the wavelenght is $\lambda_{01} = 1.64R$.

[5] Ibrahim R., Liquid Sloshing Dynamics, Cambridge University Press, United Kingdom, 2005

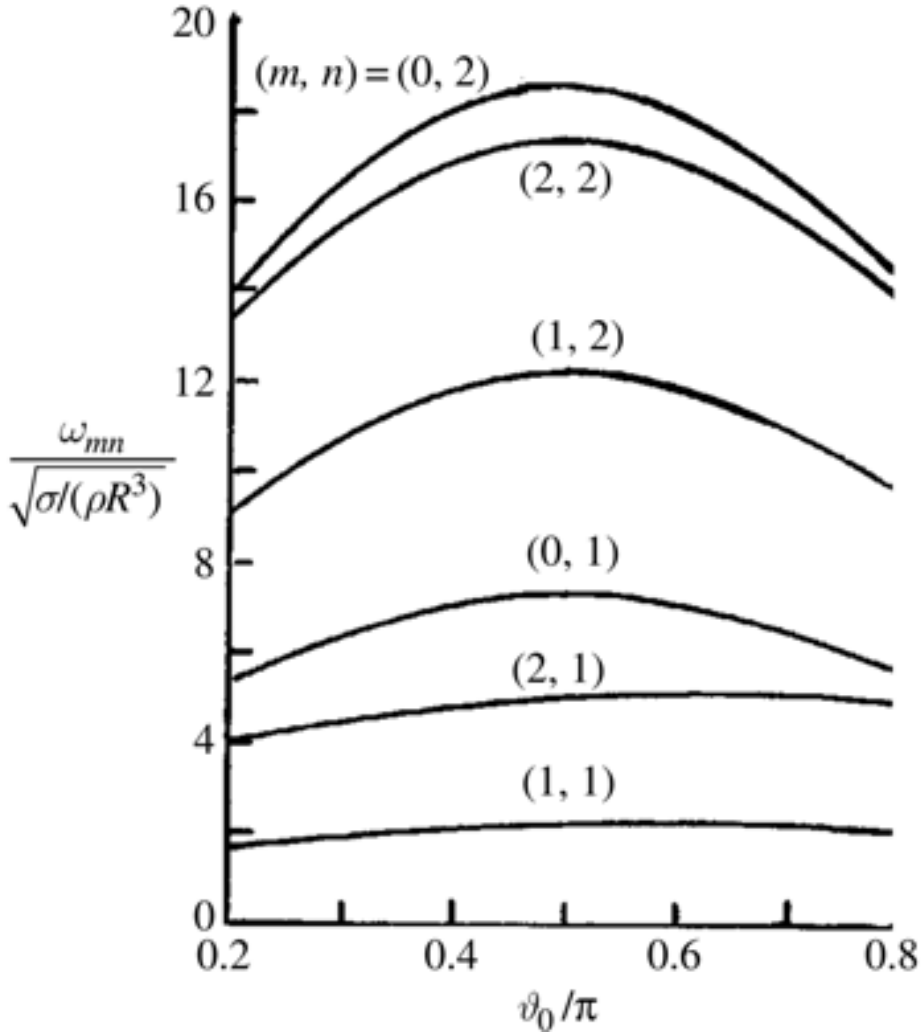

Figure 8: Natural frequencies as a function of contact angle, here ϑ_0, from Ibrahim 2005, p. 767, original data from Bauer and Eidel 1990. The non-dimensional value for mode (0,1) is $\omega^*_{01}(\vartheta_0/\pi = 0.5) = 7.36$.

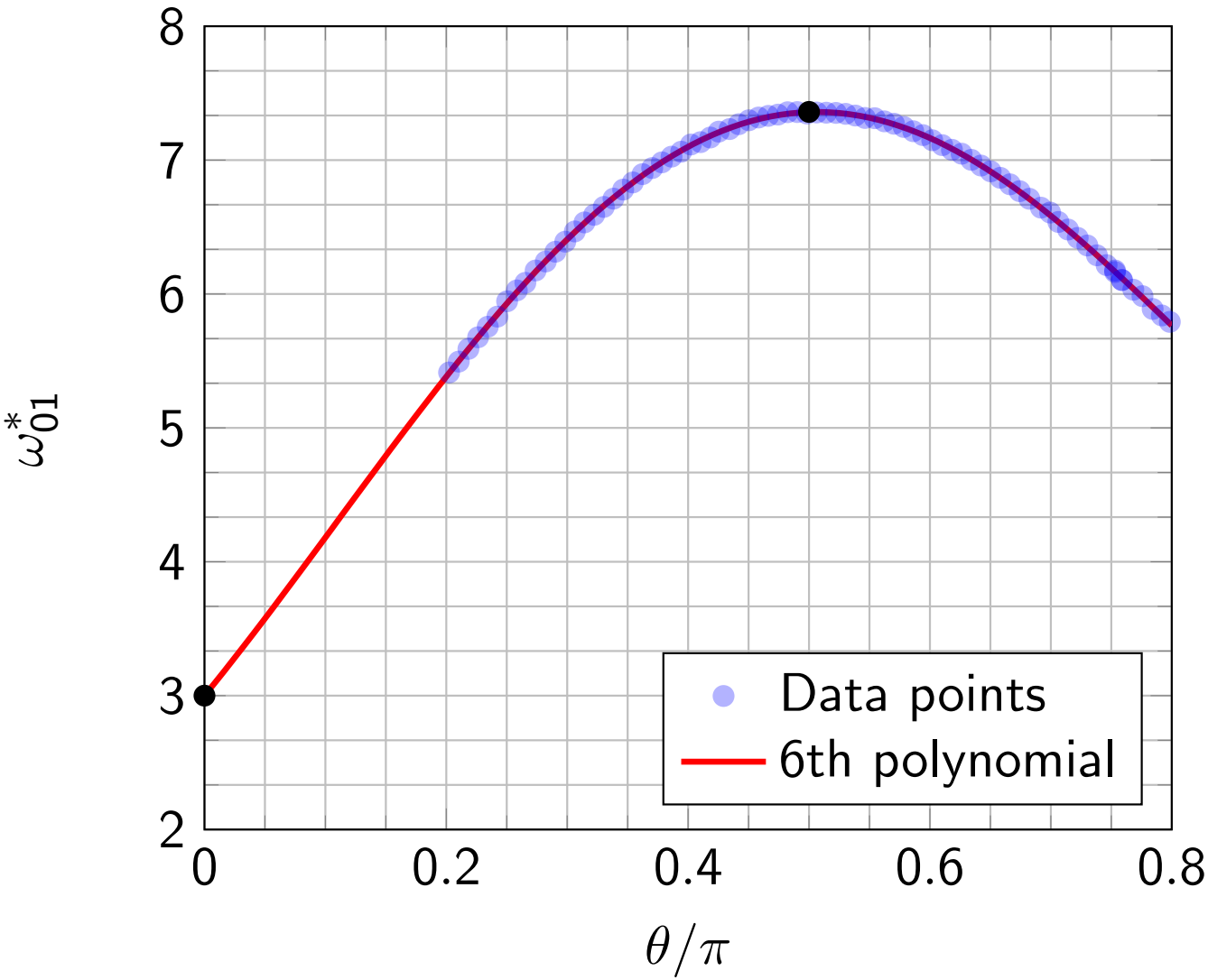

Figure 9: Reproduction from Bauer and Eidel 1990 using WebPlotDigitizer and an extrapolation a polynomial of degree six, giving $\omega_{01}^*(0) = 3$.

No data is available for a contact angle $\theta = 0$. Our guess from an extrapolation with a polynomial of degree six is $\omega_{01}^* = 3$. We will see later that this fits to our experiments. The corresponding value for the eigenvalue is $\epsilon_{01} = 2.1$.

The term ϵ_{01}/R can be seen as a wavenumber k_{01}. The wavelength can be computed from

$$k_{01} = \frac{2\pi}{\lambda_{01}} \tag{28}$$

to

$$\lambda_{01} = \frac{\pi}{\epsilon_{01}} 2R = 3.0\, R \tag{29}$$

with a wavelength $\pi/2.1 = 1.5$ times the diameter; The smaller the contact angle (for $\theta < \pi/2$), the larger the wavelength. We emphasize here, that the wavelength, and therefor the natural frequency depends on the contact angle.

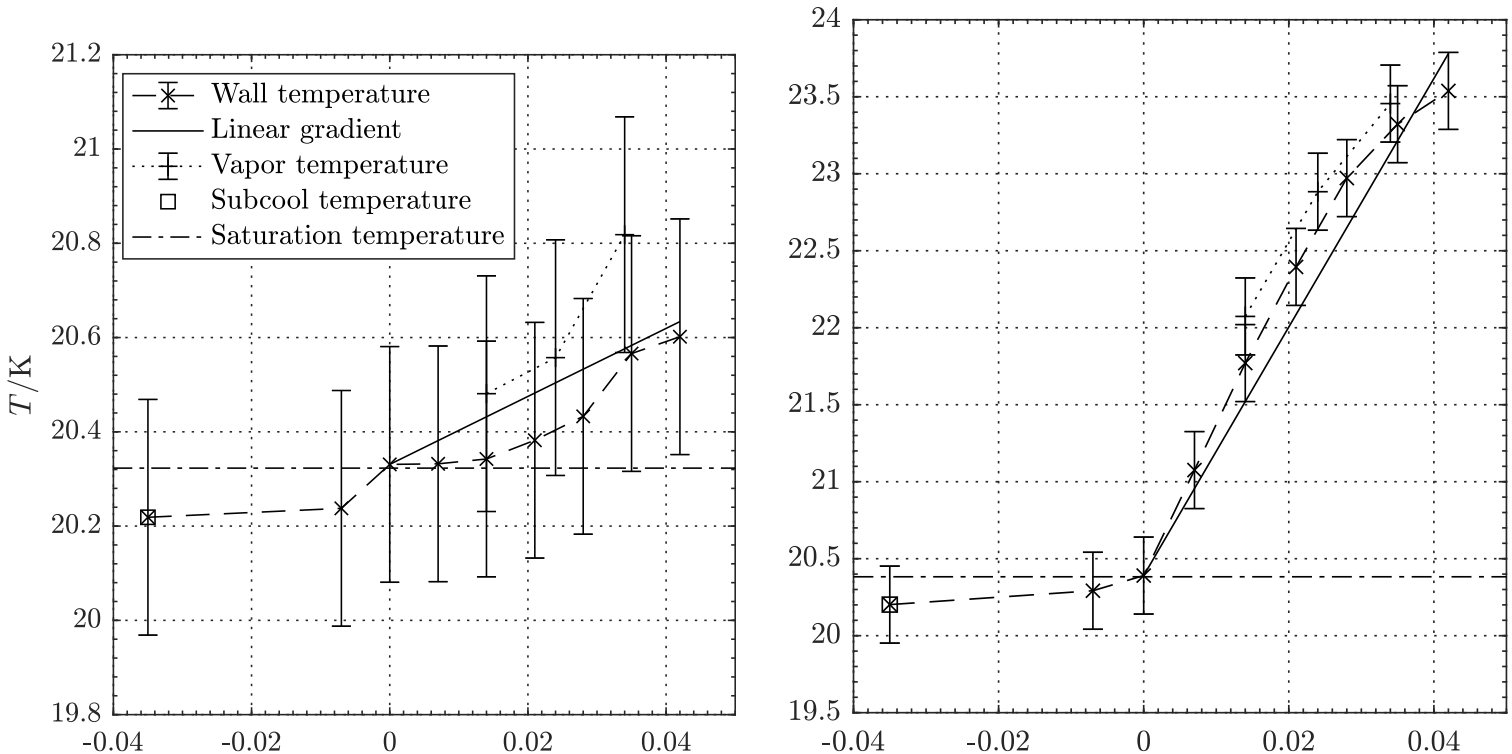

(a) $R = 26.2\,\mathrm{mm}$, isotherm (b) $R = 20.15\,\mathrm{mm}$, $80.7\,\mathrm{K\,m^{-1}}$

Figure 10: Temperature gradient along the wall in z direction (in m). $z = 0$ is the position of the sensor $\mathrm{T_{wif}}$

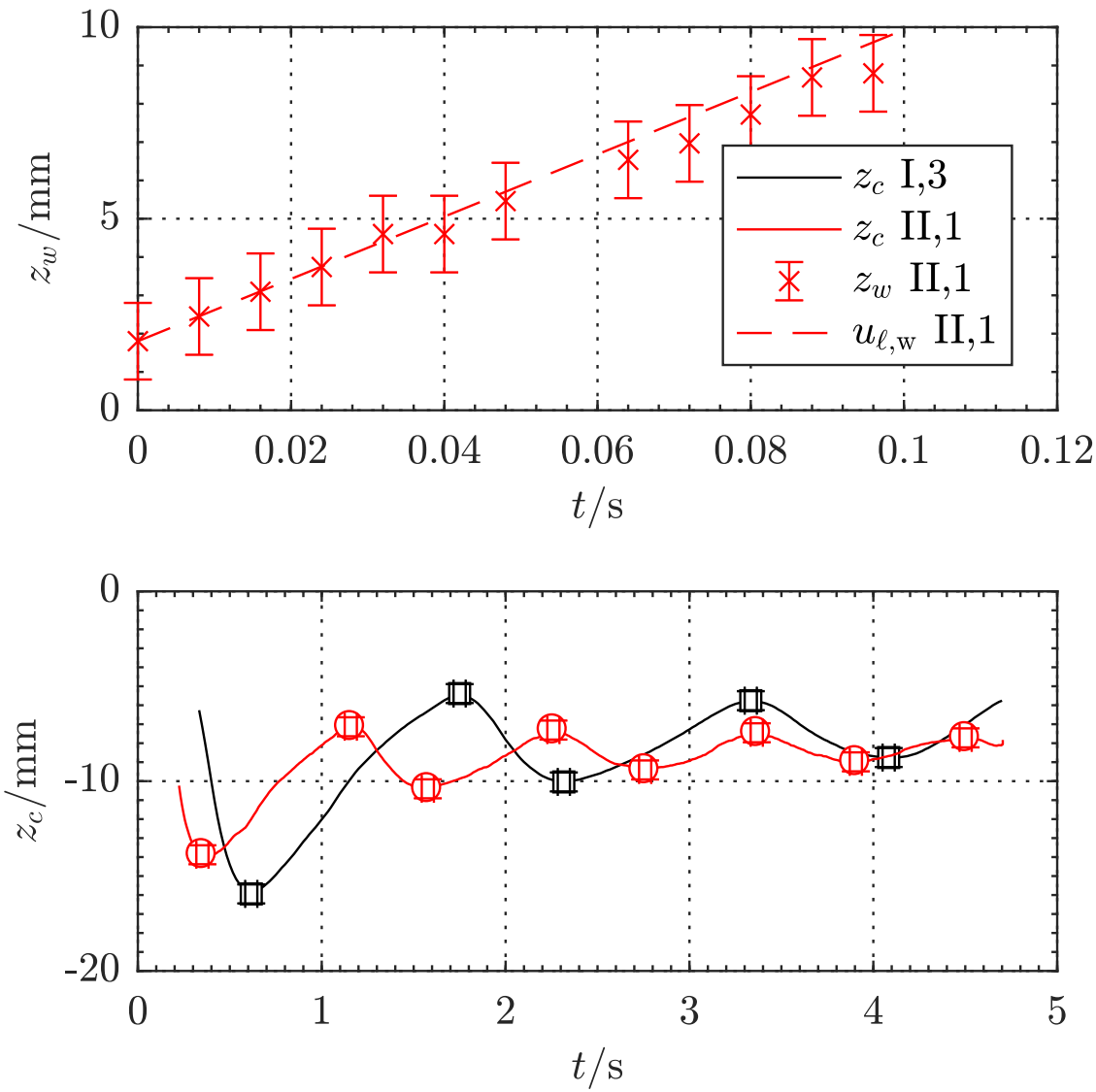

Figure 11: Isothermal: (Top) Wall line progression for $R = 20.15\,\mathrm{mm}$. (Bottom) Center point progression for $R = 20.15\,\mathrm{mm}$ (red) and for $R = 26.2\,\mathrm{mm}$ (black).

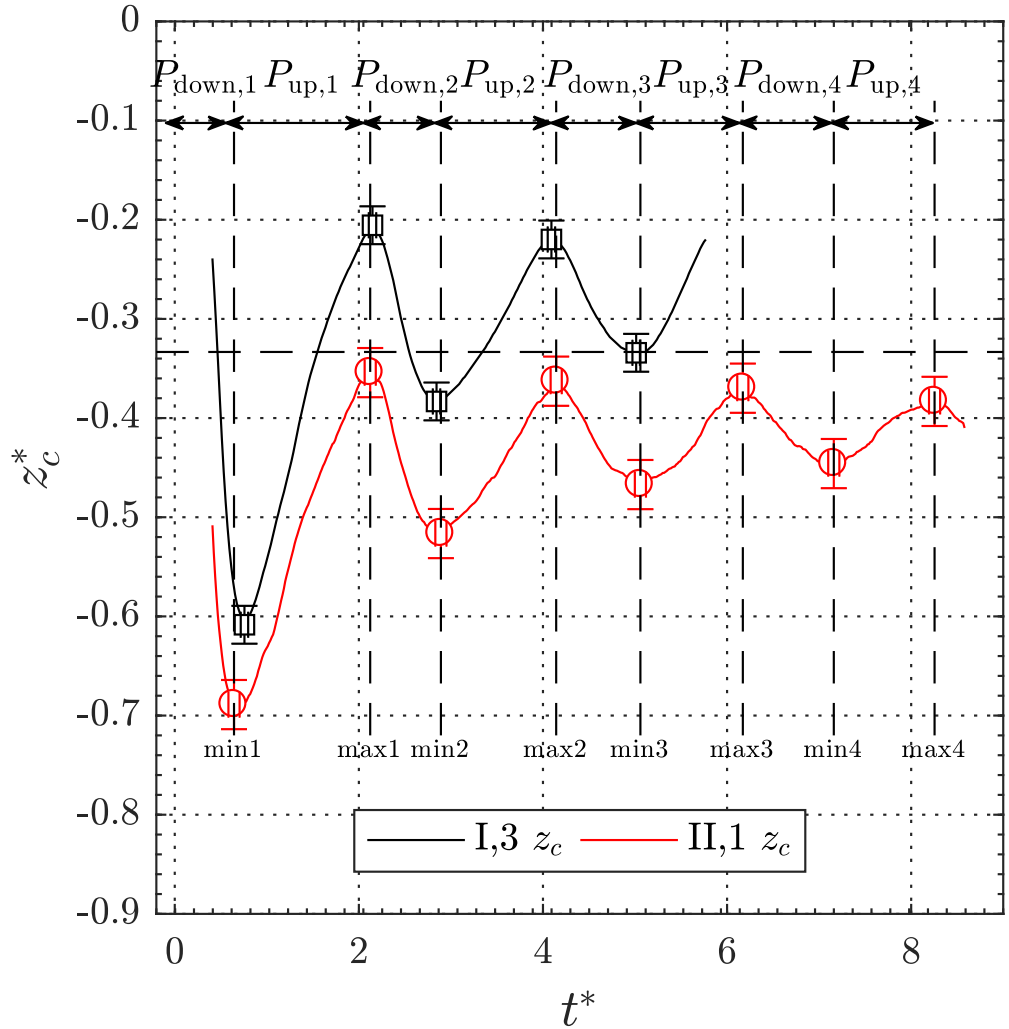

Figure 12: Center point progression of two isothermal experiments with $R = 26.2\,\text{mm}$ (black) and $R = 20.15\,\text{mm}$ (red). $z_c^* = z_c/R$ and set to initial liquid height, $t^* = t/t_{c2}$.

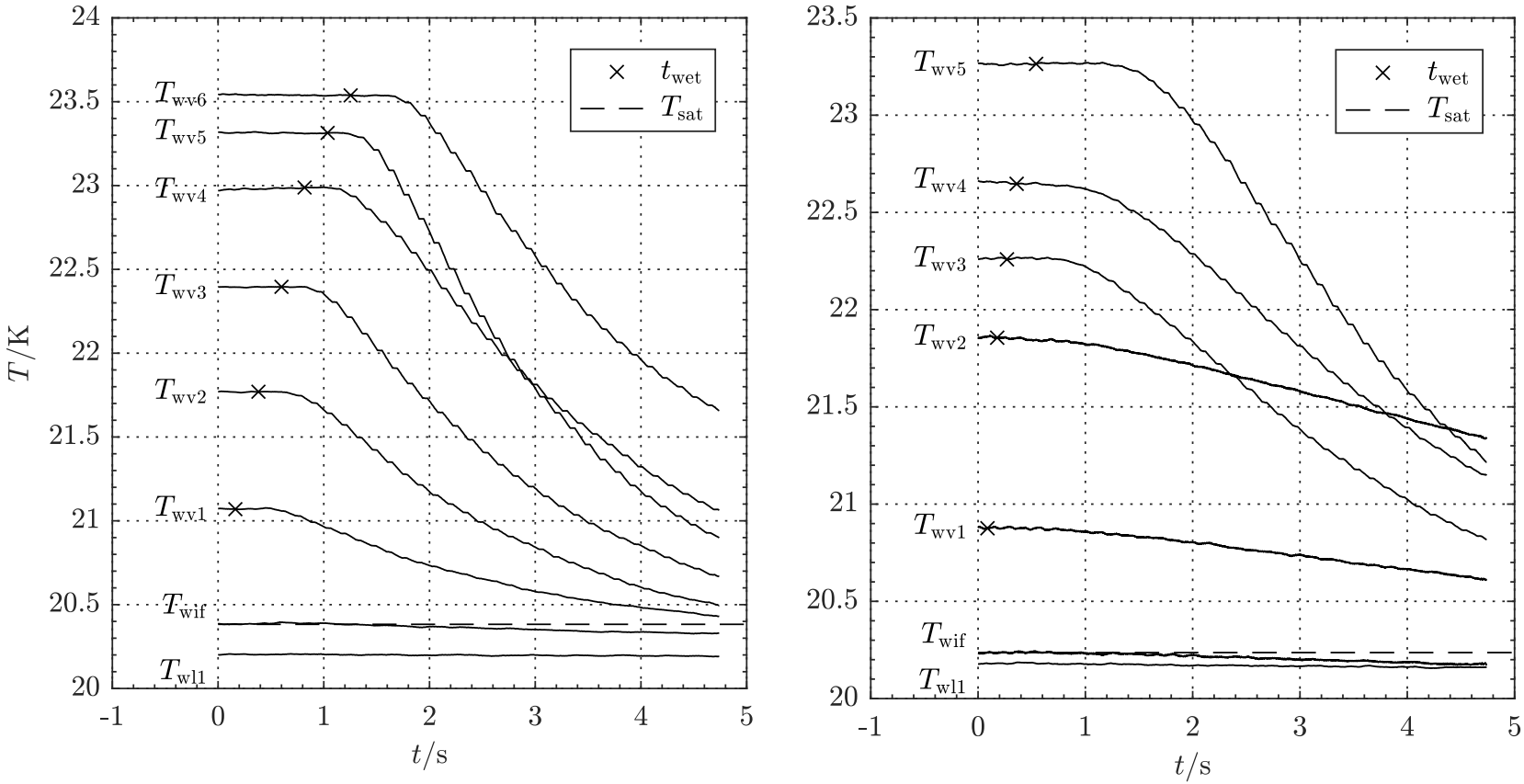

(a) $R = 26.2\,\text{mm}$, $80.7\,\text{K}\,\text{m}^{-1}$ (b) $R = 20.15\,\text{mm}$, $101.4\,\text{K}\,\text{m}^{-1}$

Figure 13: Wall temperature versus time. The crosses mark the arrival of the contact line at the position of the respective sensors. The delay time is due to temperature diffusion through the solid.

We need a few definitions before we continue: time and velocity scales

$$t_{c2} = \left(\frac{\rho_L R^3}{\sigma} \right)^{1/2} \qquad (30)$$

$$v_{c2} = \left(\frac{\sigma}{\rho_L R} \right)^{1/2} = \frac{R}{t_{c2}} \qquad (31)$$

natural frequency and half period

$$\omega = \frac{\pi}{P} = 2\pi f \qquad (32)$$

dimensionless form

$$P^* = \frac{P}{t_{c2}} \quad \omega^* = t_{c2}\omega \qquad (33)$$

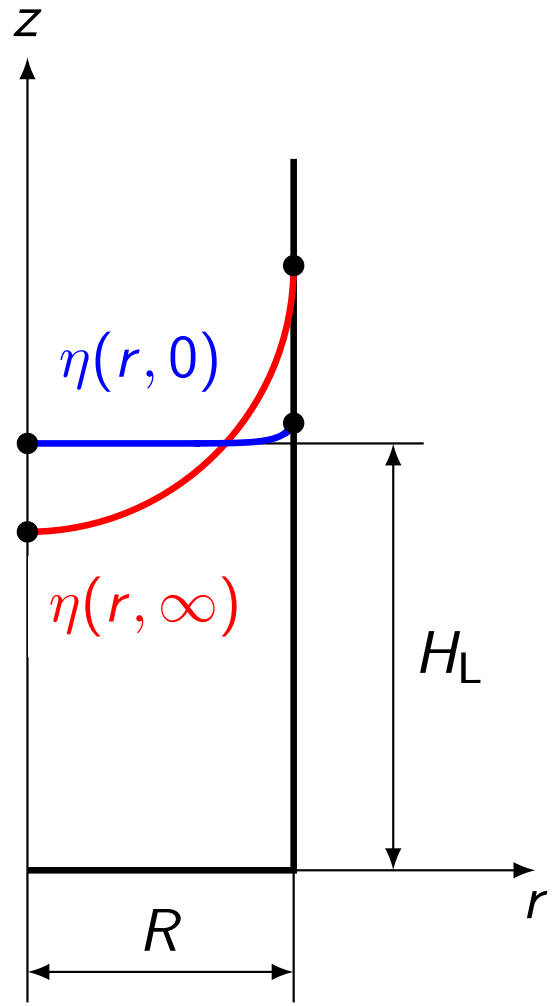

Figure 14: Initial $\eta(r, 0)$ and final $\eta(r, \infty)$ interface contour

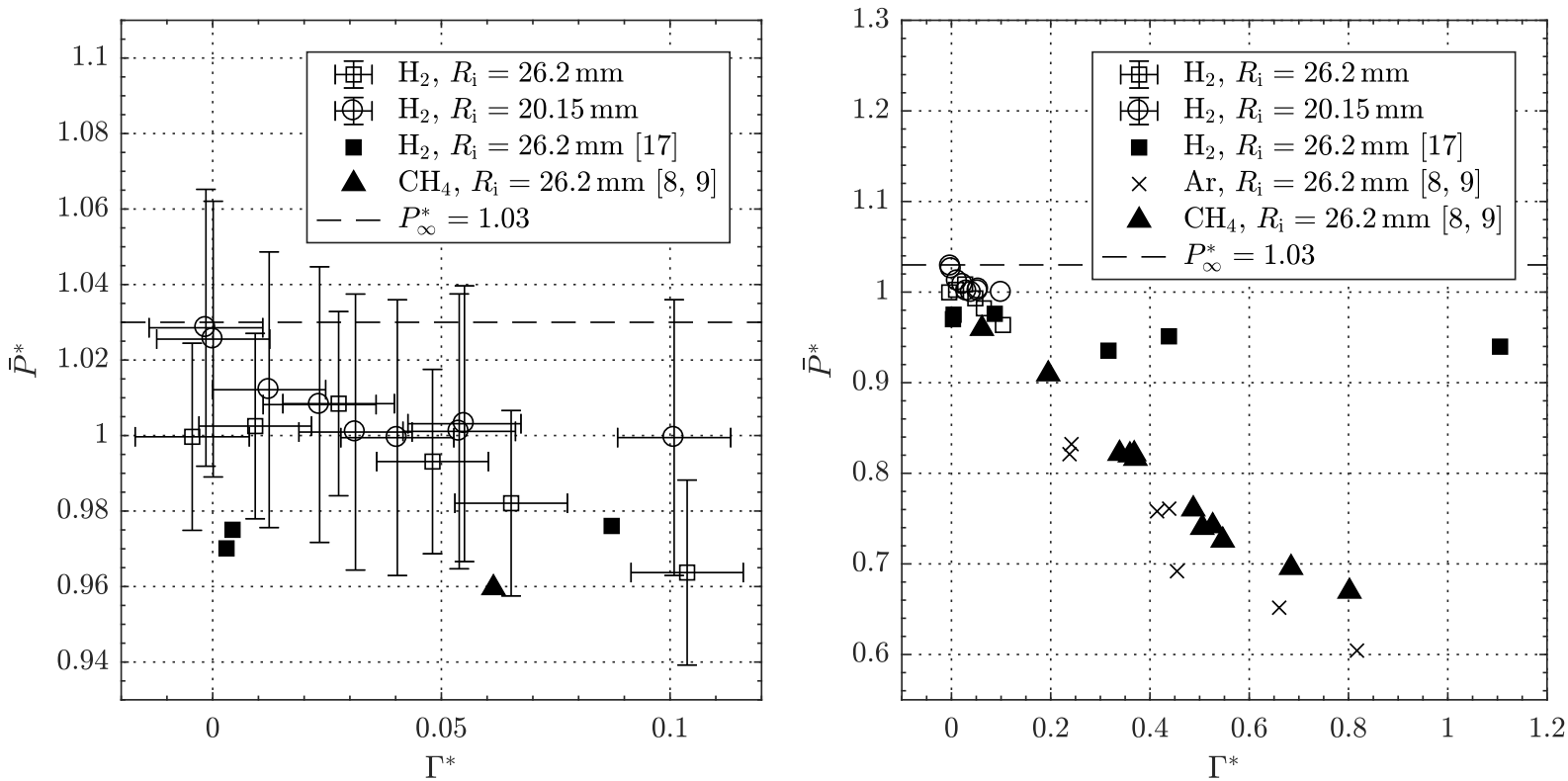

Figure 15: Dimensionless sloshing half period for two different diameters and three different fluids (Hydrogen, Argon, Methane). Data [17] from Schmitt and Dreyer 2015[6], data [8] from Kulev et al. 2014[7]. Γ^* is the dimensionless linear wall temperature gradient.

[6] Schmitt, S. and Dreyer, M. Cryogenics 72(1), 2015

[7] Kulev et al., Cryogenics 62, 2014

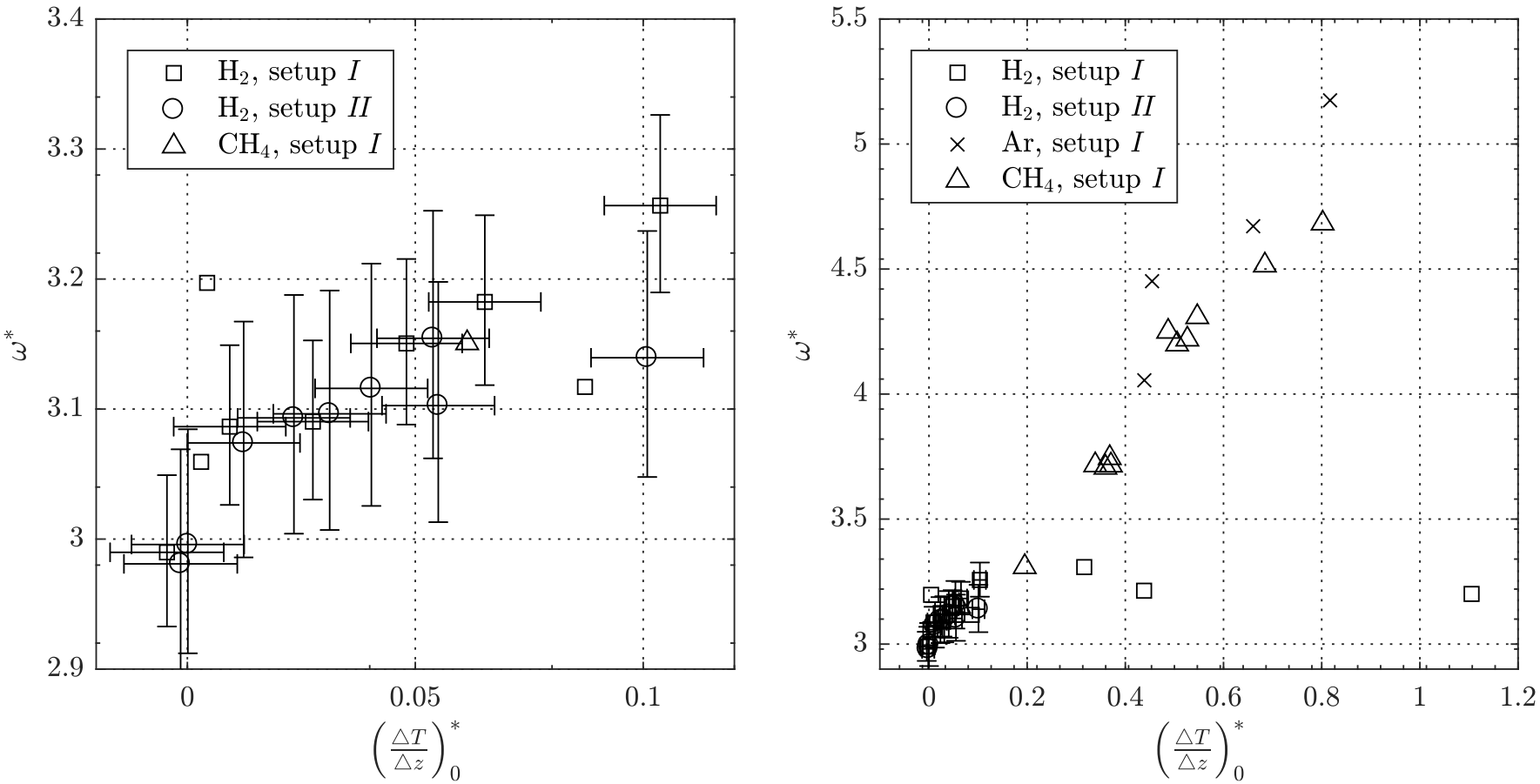

Figure 16: Dimensionless natural frequency for two different diameters and three different fluids (Para-Hydrogen[8], Argon, Methane[9]). The x-axis scale is $(\triangle T/\triangle z)_0^* = [T(z = H_\mathsf{L} + R)]/T_\mathsf{sat}$ at $(t = 0)$.

[8] Schmitt and Dreyer, Cryogenics 72, 2015

[9] Kulev et al., Cryogenics 62, 2014

We summarize our findings so far:

1. The wall superheat does not remain constant during the course of the test (5 s).
2. The temperature change of the wall can be used to compute the heat flux, and with some further assumptions the evaporative mass flux.
3. We have set up a single sided model based on the heat conduction in the wall, applying appropriate boundary conditions at the inner wall (Dirichlet) and the outer wall (Neumann, no gradient, adiabatic).

We follow the hypothesis that the change in frequency is caused by a change of the apparent contact angle θ_{app} which is affected by the evaporative mass flux. I will outline the single-side model to calculate the wall heat flux and the resulting evaporative mass flux[10].

[10] Friese/Hopfinger/Dreyer, Exp. Thermal Fluid Sci 106, 2019

Single-sided model

1. Slice the container wall into horizontal discs (here 0.5 mm), adiabatic in z-direction
2. Solve
$$\frac{\partial^2 T_S}{\partial r^2} - \frac{1}{D_{TS}} \frac{\partial T_S}{\partial t} = 0 \tag{34}$$
and assume 2D instead of 2D rot (wall thickness to radius ratio small 1/10)
3. The inner wall temperature drops from its initial value to the saturation temperature of the fluid when the liquid meniscus reaches the respective layer.
4. The outer wall is treated as adiabatic too.
5. The thermophysical properties of the solid are considered as temperature dependent.
6. Compute the temperature distribution in the solid $T_S(r, z, t)$[11]

[11] Baehr/Stephan, Waerme- und Stoffuebertragung, 2013, 2.3.3. Der einseitig unendlich ausgedehnte Koerper

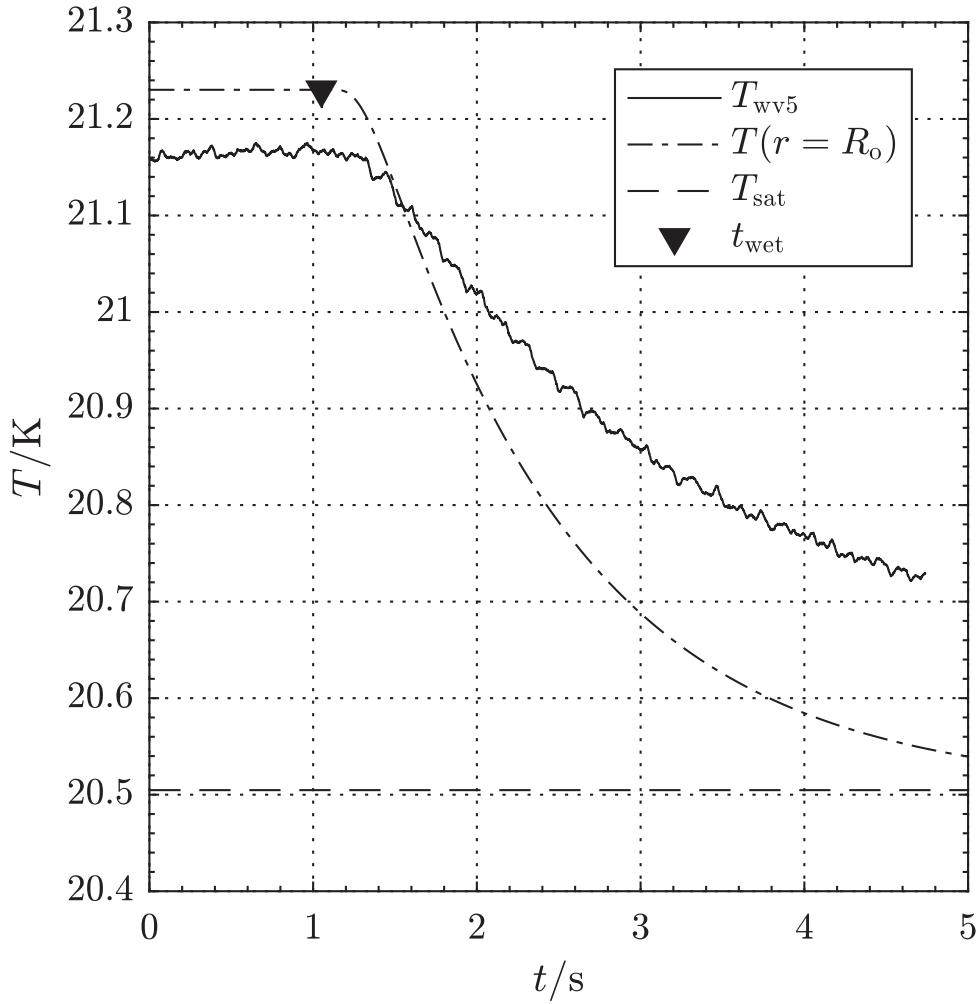

Figure 17: Temperature reading of a sensor (solid) at 37 mm above the initial liquid surface in comparison with the analytical solution (dash-dotted). The leading edge reaches this height after 1.05 s. A contact resistance exits between the sensor and the wall.

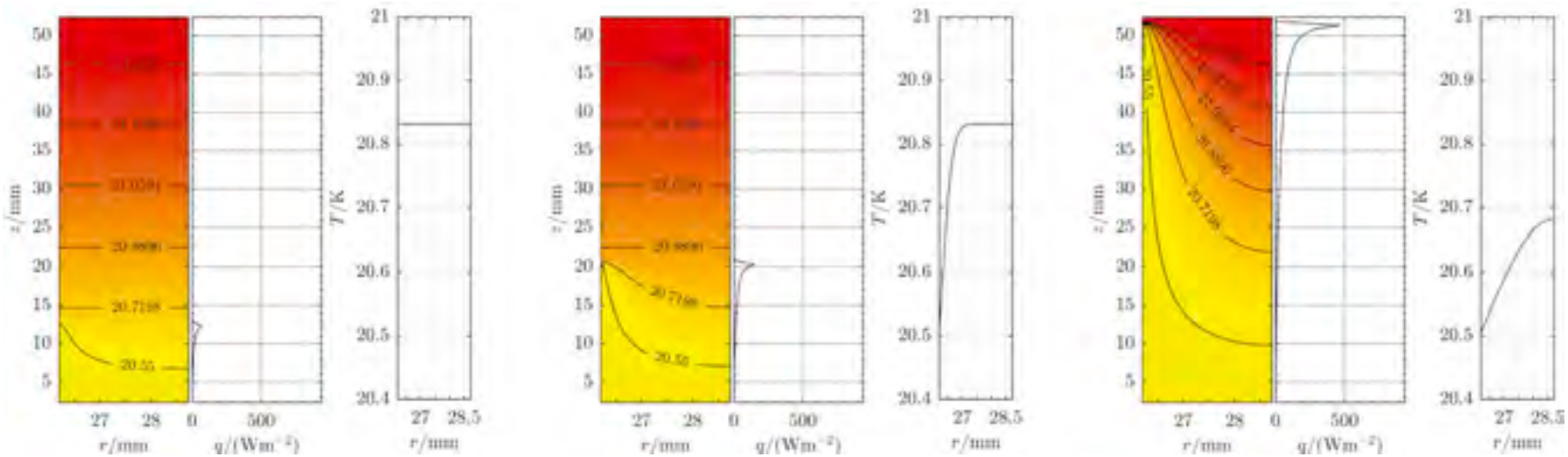

(a) $t = 0.25\,\mathrm{s}$ (b) $t = 0.5\,\mathrm{s}$ (c) $t = 1.47\,\mathrm{s}$

Figure 18: Temperature distribution, height dependent heat flux from the solid to the liquid, and the temperature profile at $z = 2R/3$. The leading edge causes the highest heat flux.

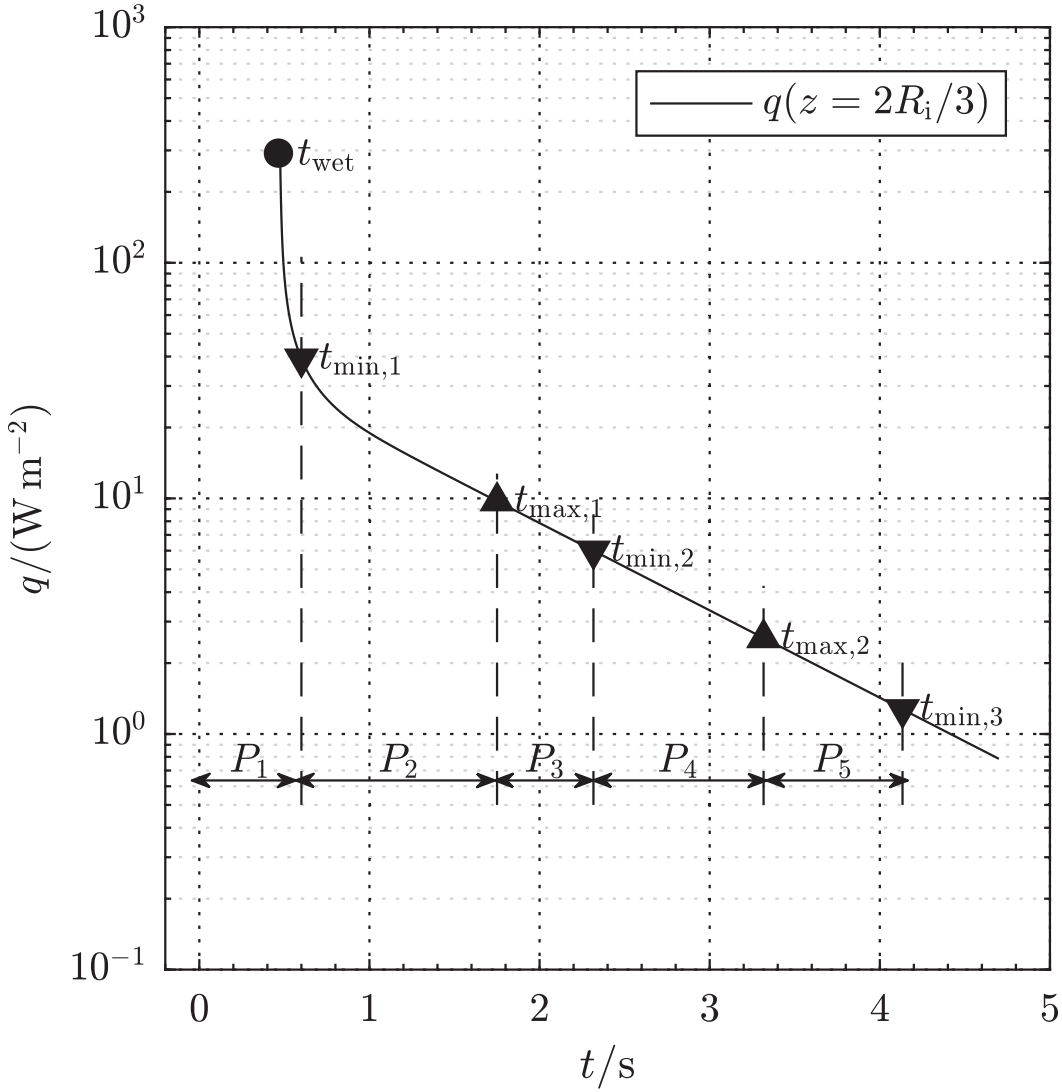

Figure 19: Wall heat flux versus time for $z = 2R/3$. The initial peak at 0.48 s is followed by an exponential decline.

Further assumptions:

1. The liquid is at saturation temperature and cannot be superheated.
2. The heat flux leads to evaporation only:

$$\dot{m} = \frac{\dot{q}}{(\triangle_{\mathrm{LG}} h)} \tag{35}$$

3. The evaporated mass per unit area is

$$m = \int_{t_1}^{t_2} \dot{m} \, \mathrm{d}t \tag{36}$$

4. The time intervals are chosen from one extremum of the center point to the next. Down in the center $\bigtriangledown$ corresponds to up at the wall (advancing contact line), and up in the center $\triangle$ corresponds to down at the wall (receding contact line).
5. The location for the analysis is at $2R/3$ above the initial surface, thus the locus of the final equilibrium contact line, if any.

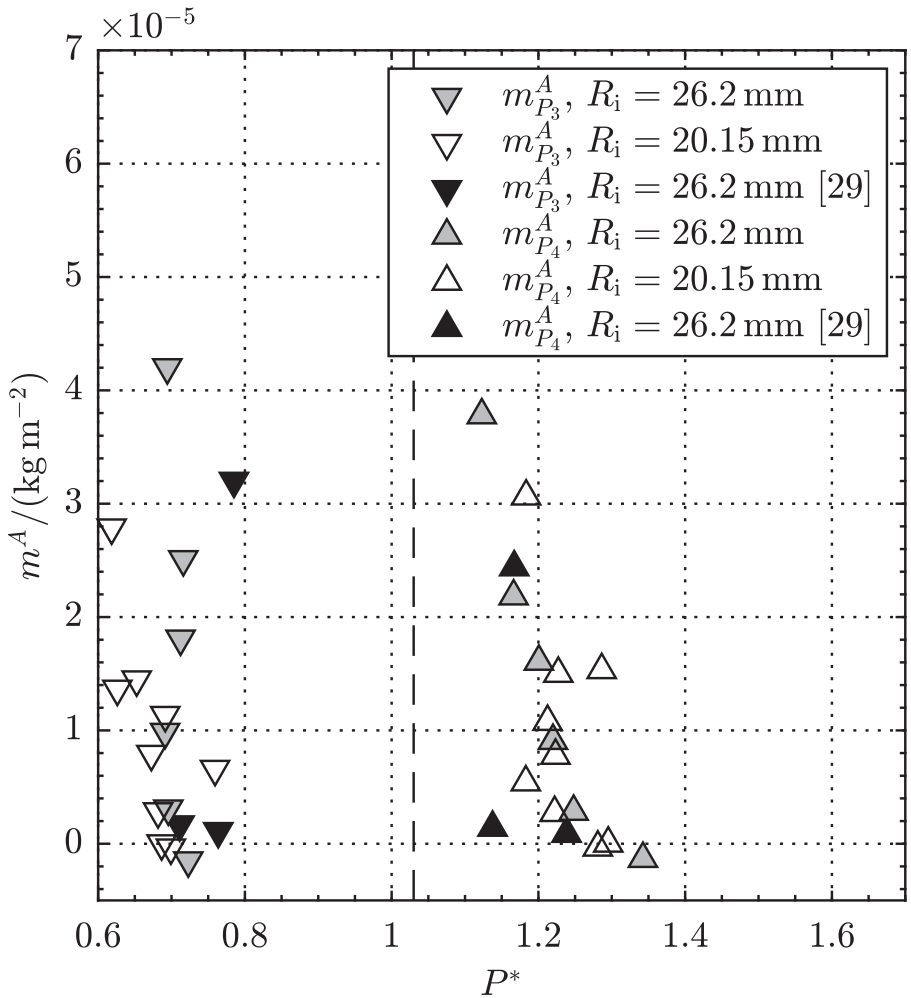

Figure 20: Evaporated mass per unit area for the first maximum to the second minimum $\bigtriangledown$ (P_3), and the second minimum to the second maximum $\bigtriangleup$ (P_4). The near wall region of the interface moves upwards for P_3 (advancing) and downwards for P_4 receding.

1. The periods of the down strokes are always smaller (higher frequency) than the periods of the upstrokes.
2. No clear dependence between the half period and the phase change mass per unit area could be found.
3. The phase change masses are similar, but the time intervals are different. This means that the phase change mass flux is higher for the down strokes of the center point, or the upstrokes of the contact line region.
4. We are not able to define a mass transfer interface in order to give the evaporated mass. Numerical calculations are needed to resolve this issue.
5. The pressure increase in the experiment is too small to compare evaporation rates from the test with the model. This is true for hydrogen only. Methane shows a clear correlation between the direction of the contact line region motion and rate of pressure increase[12].

[12] Kulev et al., Cryogenics 62, 2014

We acknowledge the funding by the German Aerospace Center (DLR e.V.) through grant number 50RL1621, and the help of our technical staff Peter Prengel and Frank Ciecior.

For further information see: Peter S. Friese, Emil J. Hopfinger, Michael E. Dreyer, Liquid hydrogen sloshing in superheated vessels under microgravity, Experimental thermal and fluid science 106 (2019) 100 - 118